AGU ADVANCING EARTH AND SPACE SCIENCE

Geophysical Research Letters

RESEARCH LETTER
10.1029/2022GL102426

Internal Gravity Waves Generated by Subglacial Discharge: Implications for Tidewater Glacier Melt

J. M. Cusack[1,2], R. H. Jackson[2], J. D. Nash[1], E. Skyllingstad[1], E. C. Pettit[1], D. A. Sutherland[3], R. J. Motyka[4,5], and J. M. Amundson[5]

[1]College of Earth, Ocean, and Atmospheric Sciences, Oregon State University, Corvallis, OR, USA, [2]Rutgers, The State University of New Jersey, Corvallis, OR, USA, [3]University of Oregon, Corvallis, OR, USA, [4]University of Alaska Fairbanks, Juneau, AK, USA, [5]University of Alaska Southeast, Juneau, AK, USA

Abstract Submarine melting has been implicated in the accelerated retreat of marine-terminating glaciers globally. Energetic ocean flows, such as subglacial discharge plumes, are known to enhance submarine melting in their immediate vicinity. Using observations and a large eddy simulation, we demonstrate that discharge plumes emit high-frequency internal gravity waves that propagate along glacier termini and transfer energy to distant regions of the terminus. Our analysis of wave characteristics and their correlation with subglacial discharge forcing suggest that they derive their energy from turbulent motions within the discharge plume and its surface outflow. Accounting for the near-terminus velocities associated with these waves increases predicted melt rates by up to 70%. This may help to explain known discrepancies between observed melt rates and theoretical predictions. Because the dynamical ingredients—a buoyant plume rising through a stratified ocean—are common to many tidewater glacier systems, such internal waves are likely to be widespread.

Plain Language Summary Recent acceleration in sea-level rise has been attributed to the mass loss of glaciers that terminate in the ocean, such as those found in Greenland and Alaska. Warm ocean currents are thought to melt glacier ice, contributing to their loss of mass and retreat. We use moored instruments deployed with autonomous vehicles, as well as a computer simulation, to demonstrate how a previously unconsidered type of current, called an internal wave, is generated at marine-terminating glaciers. We show that the strength of the waves is related to the amount of subglacial discharge that originates from surface melting occurring at higher elevations on the glacier. Internal waves may contribute to local ice melt, and ultimately glacier mass loss, by mixing warm water in a thin layer immediately adjacent to the glacier.

Key Points:

- First-ever time series of water velocity in the calving zone of a glacier terminus, enabled by moorings deployed from a robotic vessel
- Energetic high-frequency internal waves were emitted from the subglacial discharge plume and reproduced in a large eddy simulation
- Internal waves have the potential to significantly increase ambient melt rates by enhancing water velocity across the terminus

Supporting Information:

Supporting Information may be found in the online version of this article.

Correspondence to:

J. M. Cusack,
jesse.cusack@oregonstate.edu

Citation:

Cusack, J. M., Jackson, R. H., Nash, J. D., Skyllingstad, E., Pettit, E. C., Sutherland, D. A., et al. (2023). Internal gravity waves generated by subglacial discharge: Implications for tidewater glacier melt. *Geophysical Research Letters*, *50*, e2022GL102426. https://doi.org/10.1029/2022GL102426

Received 9 DEC 2022
Accepted 1 MAR 2023

1. Introduction

Fjords with active tidewater glaciers are principle conduits for meltwater runoff and ice discharge into the ocean. Tidewater glaciers have been losing mass in recent years and contributing to an acceleration in sea-level rise (Chambers et al., 2017; Mouginot et al., 2019; Rignot & Kanagaratnam, 2006; Shepherd et al., 2020). The ocean dynamics occurring within glacial fjords play a key role in modulating glacier retreat (Straneo & Cenedese, 2015; Wood et al., 2018). Ocean thermal forcing directly causes mass loss via melting and may also act to amplify other ice-loss mechanisms such as calving (Luckman et al., 2015; Slater et al., 2021), although there is uncertainty in the sign and magnitude of this effect (Ma & Bassis, 2019; Mercenier et al., 2020). Increasing meltwater runoff has been linked to a weakening of the Atlantic Meridional Overturning circulation in recent decades (Thornalley et al., 2018).

Since direct observations of submarine melting are scarce, melt rates are often estimated from near-terminus ocean velocity, temperature, and salinity using a parameterization for heat and salt fluxes through the ocean boundary layer. The most widely used form of the parameterization, known as the 3-equation model, assumes shear-driven boundary layer dynamics in which the heat and salt fluxes are linearly dependent on the terminus-parallel ocean velocity (Holland & Jenkins, 1999; Jenkins, 2011, and Text S1 in Supporting Information S1). The 3-equation model suggests that the melt rate m is proportional to:

$$m \propto C_D^{\frac{1}{2}} \Gamma_T |\boldsymbol{u}| \Delta T, \quad (1)$$

where C_D is the drag coefficient, Γ_T is the turbulent thermal transfer parameter, $\boldsymbol{u}$ is the terminus-parallel outer boundary layer velocity, and ΔT is the temperature difference across the boundary layer. Parameterized melt rates are often coupled with theory for buoyant plumes (Jenkins, 2011; Morton et al., 1956) and have been used to model the melt rates of subglacial discharge plumes (Carroll et al., 2016; Cowton et al., 2015; Slater et al., 2015, 2022), which are highly energetic buoyant flows commonly found at tidewater glaciers. These discharge plumes rise from the glacier grounding line and originate from upstream surface meltwater that has drained to the glacier bed and flowed downslope via a network of subglacial channels. Measurements of terminus morphology suggest that melt induced by discharge plumes is large (Fried et al., 2015, 2019; Rignot et al., 2015; Sutherland et al., 2019), consistent with solutions to Equation 1 for high-velocity flows.

Away from the main subglacial discharge plume(s), coupled plume-melt theory suggests that the buoyant forcing from melt alone drives relatively weak plumes (Cowton et al., 2015; Magorrian & Wells, 2016; Straneo & Cenedese, 2015). As such, melting occurring away from discharge plumes, termed ambient melting, was thought to be small.

Yet, the only direct observations of submarine melting made to date demonstrate that ambient melting exceeds theoretical estimates by one to two orders of magnitude (Sutherland et al., 2019). Reasons for this discrepancy include: incorrect values for the drag and turbulent transfer coefficients, an incorrect form of the parameterization at low velocity (McConnochie & Kerr, 2017; Schulz et al., 2022) and the neglect of non-plume flows from the assumed near-terminus ocean velocity, such as those from lateral fjord-circulation (Jackson et al., 2020; Slater et al., 2018). Here, we focus on additional sources of near-terminus currents that could contribute to enhancing melt, in particular, energetic internal waves revealed by a new set of observations.

Throughout the ocean, internal gravity waves are a dominant source of energy for turbulent mixing and exert significant influence over a diverse range of processes from nutrient availability to the global overturning circulation (MacKinnon et al., 2017; Melet et al., 2013; Woodson, 2018). Winds and tides are the main energy sources for internal waves in the global ocean (Ferrari & Wunsch, 2009), while isolated buoyant plumes common to glacial fjords have not previously been identified as a wave source. In the ocean, only horizontally propagating plumes from rivers have been linked to internal wave generation (Nash & Moum, 2005). In the atmosphere, convective plumes associated with thunderstorms are known to generate internal waves (Clark et al., 1986; Fovell et al., 1992; Lane et al., 2001; Yue et al., 2013). Internal waves are commonly observed in fjords and typically develop from tidal flows over sills (Bourgault et al., 2011; Farmer & Armi, 1999; Farmer & Smith, 1978; Gillibrand & Amundrud, 2007; Ross et al., 2014). Very recent observations from the Antarctic Peninsula suggest that iceberg calving events are also a source of internal waves and significant mixing (Meredith et al., 2022).

Propagating internal waves have an upper frequency limit equal to the local buoyancy frequency, N, which ranges from around 24 cycles per day (cpd) in the deep ocean to well over 100 cpd in highly stratified locations, such as fjords. Winds and tides typically excite waves at frequencies much lower than N ($\leq$2 cpd), while nonlinear wave interactions facilitate energy transfers to higher frequencies. In the laboratory, plumes and mechanically generated turbulence have been demonstrated to generate near-N waves (Ansong & Sutherland, 2010; Dohan & Sutherland, 2005).

While internal gravity waves are ubiquitous in stratified fluids, they have not been observed near the ice-ocean interface of tidewater glaciers. This is due in part to the difficulty involved in collecting measurements close to the calving termini of glaciers, which must be done using autonomous or remotely operated platforms. Furthermore, moving instruments tend to alias temporal and spatial signals, making it difficult to detect propagating waves. Moored instruments anchored to the seafloor are better able to isolate oscillatory signals but are at significant risk of being destroyed by icebergs and are typically deployed from ships that cannot approach close to glacier termini. Past moored records have been located greater than 1 km from glacier termini, and have generally aimed for long-duration records, necessitating low-frequency sampling that may not detect high-frequency waves (Jackson et al., 2014; Moffat, 2014).

Here, we present the first-ever time series of ocean velocity within the calving zone of a tidewater glacier. Our observations reveal that energetic internal waves account for nearly half of the near-terminus velocity variability and could significantly enhance melt rates. We are able to reproduce the wave characteristics accurately in an idealised numerical simulation forced only by a subglacial discharge plume. Because discharge plumes are a ubiquitous feature of tidewater glacier systems, such internal waves may be common.

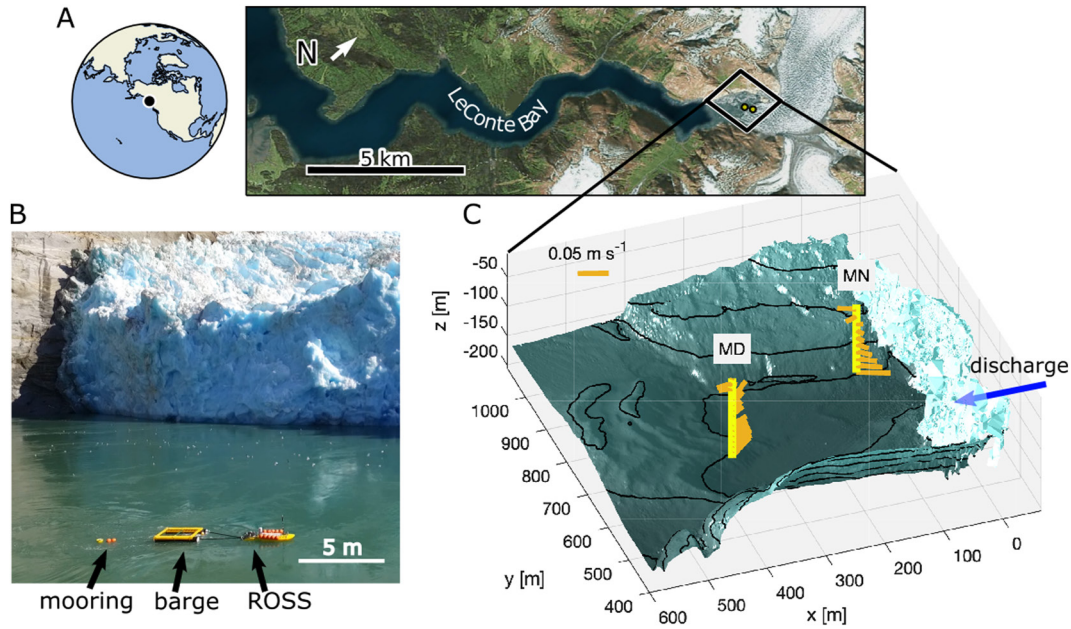

Figure 1. (a) Map of LeConte Bay, located in Southeast Alaska. The study region is located at the end of the bay in the boxed region. (b) Remote deployment of a mooring captured from drone footage. (c) A 3-D view of the observed bathymetry and glacier morphology looking down at the fjord from the southwest. Mooring locations are denoted by yellow bars and mean velocity vectors are given by orange quivers. The approximate location of the discharge outlet is indicated with an arrow.

2. Materials and Methods

In September 2018, an extensive dataset of near-terminus ocean properties were collected during a field campaign at LeConte Glacier (Xeitl S´ıt' in Tlingit), Alaska (Figure 1a). Remotely controlled kayaks called Robotic Oceanographic Surface Samplers or ROSS (Nash et al., 2017) were used to deploy a mooring approximately 100 m from the terminus and roughly 150 m from the discharge plume source (the near mooring, MN, Figures 1b and 1c) at the beginning of the campaign (1–3 September). Uniquely, MN was instrumented with a 5 beam Acoustic Doppler Current Profiler (ADCP) providing direct measurements of vertical velocity over 13–134-m depth. A second more distant mooring (denoted MD), instrumented with two 4 beam ADCPs, was deployed by ship approximately 400 m from the terminus and discharge plume, and measured velocities from 6 to 165-m depth. A series of processing steps are applied to the ADCP data to remove noise, exclude iceberg calving events, and reduce biases, but some of horizontal velocity estimates are likely biased low due to beam spreading (Text S2, Figure S1 in Supporting Information S1). Both moorings were recovered at the end of the campaign (12–18 Sept), during which time a large number of additional observations were obtained, including ship- and ROSS-based profiles of temperature and salinity.

Complementing the in-situ observations, a large eddy simulation (LES) with a uniform resolution of 1 m was conducted to investigate plume-driven ocean variability (Figure 2a). Compared to models that have previously been used to study discharge plumes, such as MITgcm, the LES uses a sophisticated turbulence closure scheme that better represents the largest turbulent scales relevant to internal wave generation (Text S3 in Supporting Information S1). The domain is an idealized rectangular channel of width 1 km, length 6 km, and depth 165 m, approximating the dimensions of the near-terminus region at LeConte. At the eastern wall of the model (the "glacier") melting is parameterized using the 3-equation model (Holland & Jenkins, 1999). The model was initialized with a horizontally uniform, depth-dependant temperature $T(z)$ and salinity $S(z)$, and forced by 150 $m^3\ s^{-1}$ of subglacial discharge injected from a 100 m wide by 4 m high channel at the base of the eastern wall. The temperature and salinity profiles were derived from the average of 35 near-glacier CTD casts. The chosen discharge flux is close to the average for the fieldwork period (Jackson et al., 2020) and the shape of the discharge outlet is roughly based on prior inferences of subglacial outlets from glaciers in Greenland (Fried et al., 2019; Jackson et al., 2017; Slater et al., 2017). Boundary conditions at the western downstream fjord exit above 60 m depth were set to a

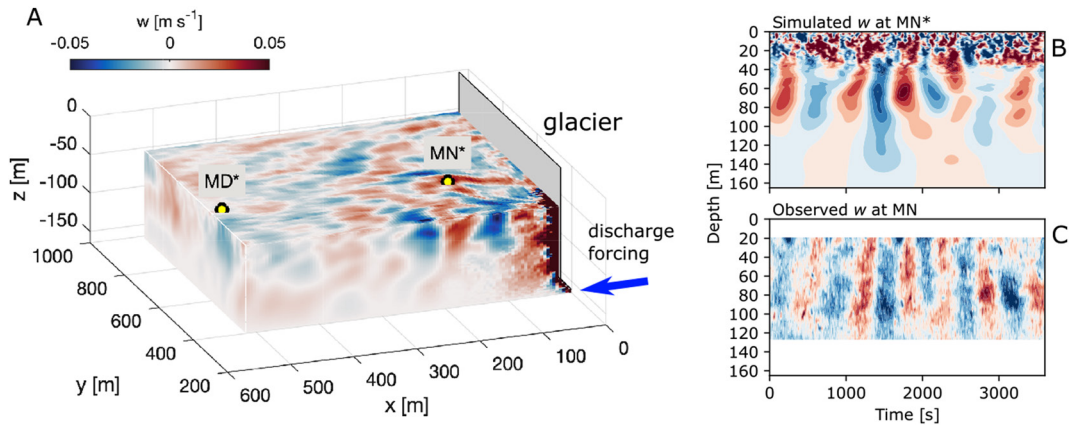

Figure 2. (a) A snapshot of the vertical velocity field from a 600 m wide subset of the 1,000 m wide large eddy simulation (LES) domain. The simulation was forced by 150 $m^3\ s^{-1}$ of freshwater injected at the location of the blue arrow. MD∗ and MN∗ represent points in the model corresponding to the real mooring locations. (b) One hour of vertical velocity output from MN in the LES. (c) Observed vertical velocity over 1 hr from mooring MN.

constant outflow equal to the total prescribed subglacial discharge influx. Below 60 m, the outflow velocity was set to zero.

3. Results

Observed and simulated vertical velocity time series confirm the presence of an energetic internal wavefield (Figure 2). The waves appear as regular bands of positive and negative vertical velocity with a period of approximately 10 min and magnitude exceeding 5 cm s^{-1}. The same regular oscillations are also observed in horizontal velocity and at the more distant mooring (Text S4 and Figure S2 in Supporting Information S1). An analysis of the dynamical wave modes using observations suggests that the dominant horizontal wavelength lies between 100 and 800 m, most likely toward the lower end of this range (Text S5 and Figure S3 in Supporting Information S1).

In the numerical simulation, waves emerge from the discharge plume and propagate throughout the fjord and along the terminus (Figure 2a, Movie S1).

The observed wave signals are superposed on a slowly varying horizontal circulation (e.g., Figure 1c) and turbulent motions confined to the upper 30 m associated with the outflowing discharge plume. The magnitude of observed horizontal velocities is less than the internal waves velocities at mid-depths (30–100-m) but exceeds the wave velocities in the shallowest and deepest parts of the water column (Figures S2a and S2b in Supporting Information S1). Variability in the surface horizontal velocity has been analyzed in prior works using iceberg tracking and autonomous boat surveys (Jackson et al., 2020; Kienholz et al., 2019). The turbulent motions are readily seen in the numerical model output (Figure 2b), but are not always apparent in the ADCP data because of the instruments' resolution and the potential for surface contamination.

Internal waves produce a peak in the vertical kinetic energy (KE) spectrum between frequencies of 50–300 cycles per day (cpd) equivalent to 5–30 min periods (Figure 3a), close to but less than the maximum observed buoyancy frequency which is ∼300 cpd. We exploit the narrow-band nature of the wave signal to study the relative energy content of waves and their impact on predicted melt rates. Specifically, we decompose the data into a high-frequency wave band (50–300 cpd), and a low-frequency band (<50 cpd) using moving averages that are robust to data gaps. The wave band isolates the most energetic internal waves but may also contain contributions from non-wave motions such as turbulence at shallow depths. The low-frequency band contains the fjord circulation, as well as low-frequency internal wave motions and tides.

The mean total KE in the wave band at mooring MN is $(2.1 \pm 0.2) \times 10^{-3}$ J kg^{-1} at 95% confidence or 42% ± 2% of the total when averaged over 20–120 m depth. The depth range chosen is the intersection of the observed depths at the two moorings allowing for a fair comparison at these two locations. At MD, which is 4 times further from the discharge source, the depth-average KE in the wave band is $(0.9 \pm 0.1) \times 10^{-3}$ J kg^{-1}, approximately half that found at MN.

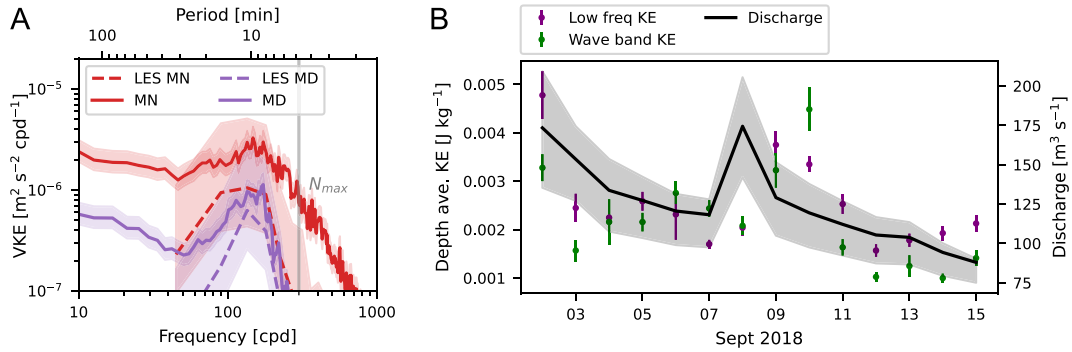

Figure 3. (a) Vertical kinetic energy (KE) spectra averaged over 30–60-m depth, where the wave signal is strongest, from mooring data (solid lines) and large eddy simulation (dashed lines). Maximum buoyancy frequency is marked with a vertical line. (b) Daily depth-averaged KE from mooring MN split into wave and low frequency components, as well as the subglacial discharge flux. In all plots the shaded regions and error bars indicate 95% confidence intervals.

Internal waves appear near-continuously throughout the observational period but with some variability in their KE (Figure 3b). We find a positive correlation (0.4 ± 0.2 at 68% confidence) between wave KE at the near-glacier mooring and the subglacial discharge flux estimated from a glacier runoff model (Amundson et al., 2020; Sutherland et al., 2019). We also find a positive correlation between low-frequency KE and discharge (0.5 ± 0.2). The short record length, inherent variability in the wave and low-frequency fields, and uncertainty in the runoff model may be reasons for the modest correlation estimates. Times of greater low-frequency KE, such as September 9–11, are associated with the presence of a strong surface outflow of subglacial discharge plume water above the mooring. Prior work has demonstrated that this outflow is often concentrated in a relatively narrow current that regularly changes orientation (Kienholz et al., 2019). The relative timing of peaks in discharge and KE hint at a 1–2 days lag between changes in runoff and changes in ocean circulation (Figure 3b), which could result from inadequate representation of water storage in the glacier runoff model (Jackson et al., 2022; Jansson et al., 2003). However, a lag-correlation analysis did not result in higher correlation estimates. Interestingly, we find a good correlation between wave and low-frequency KE (0.7 ± 0.1), which could indicate that waves derive their energy from the laterally spreading surface expression of the discharge plume, rather than its vertically rising part. Since both the rising and spreading parts ultimately derive their KE from the potential energy of the freshwater ejected at the glacier grounding line, this points to discharge as the common energy source for both low-frequency and wave band KE.

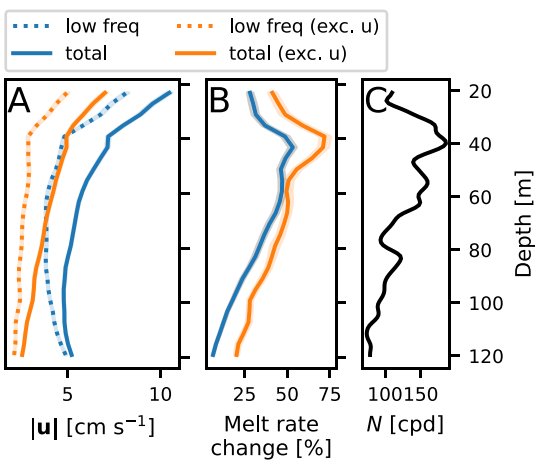

Figure 4. (a) Time-mean ocean speed at mooring MN with (solid) and without (dashed) the internal wave band. The speed is calculated in two ways: with the eastward component of velocity (blue) and without (orange). (b) Change in parameterized melt rate implied by the inclusion of wave velocities. Shading indicates the 95% confidence interval calculated using a bootstrapping procedure. (c) Average buoyancy frequency from 35 near-terminus CTD profiles.

We use Equation 1 to estimate the impact of high-frequency internal wave motions on melt rates for velocity observations at mooring MN. We estimate terminus-parallel speed in two ways, (a) using only the northward horizontal velocity component, since the glacier terminus is oriented approximately north-south and (b) using all horizontal velocity components (Figure 4a). Changes in melt rate are calculated as the ratio of speed with and without high-frequency motions. We neglect the contribution of ambient melt plumes to the velocity, since they were not measured. In both cases, the terminus-parallel mean speed is much greater when wave motions are included. For the "northward only" case, predicted melt rates above 100-m depth increase by up to 70% (Figure 4b), while for the "northward and eastward" case, they increase by up to 50%. The enhancement in melt rates is focused around the pycnocline, where buoyancy frequency is greatest (Figure 4c), consistent with the expectation from classical internal wave theory that internal wave energy scales with buoyancy frequency (Gill, 1984, Chapter 8.12.2).

4. Discussion

These new measurements from autonomously deployed moorings suggest that energetic internal waves are a persistent feature at LeConte Glacier. Our

results raise a number of questions. How ubiquitous are internal waves at tidewater glaciers? Can you predict wave amplitudes and frequency from subglacial discharge rates and ocean stratification? Tackling these broader questions will be the goal of future work. Below, we focus on two of the main questions that arise from our results, namely, how are the waves generated and what is their potential contribution to melting?

4.1. How Are the Internal Waves Generated?

A mechanism for wave generation must explain the properties of the waves found above, in particular, their near-N frequency, persistence and correlations with discharge forcing. Possible mechanisms for generating internal waves include iceberg calving (Meredith et al., 2022) and flow-topography interactions (Farmer & Armi, 1999). Additionally, internal waves may be emitted from turbulence in the rising plume, perhaps via a similar mechanism to that occurring within thunderstorms (Ansong & Sutherland, 2010; Fovell et al., 1992). The lateral outflow of plume water at the neutral buoyancy depth, which resembles a density current (Nash & Moum, 2005; White & Helfrich, 2008) or a convective boundary layer (Clark et al., 1986; Kuettner et al., 1987), could be another source of internal waves. We refer to wave generation by the plume and its lateral outflow as "turbulent emission". While calving and flow-topography interactions may generate waves and introduce variability into measurements, the numerical simulation, which lacks any of these forcings, is able to reproduce the observed wave characteristics. Calving and flow-topography interactions also cannot explain the observed correlation between waves, low-frequency KE and subglacial discharge fluxes and the persistence of the wavefield during periods of low calving activity.

We suggest that a turbulent emission mechanism may best reflect the observations. While traditional theories for discharge plumes cannot generate unsteady waves because they average out unsteady (turbulent) dynamics (Morton et al., 1956), plumes are known to be highly turbulent. Laboratory results have shown that turbulence and buoyant plumes can generate internal waves with a frequency near N (Ansong & Sutherland, 2010; Dohan & Sutherland, 2005). Additionally, the mechanism provides a dynamical connection between turbulence, horizontal fjord circulation, and internal waves that could explain the persistence of waves and the correlation among these quantities. Significantly more work is needed to confirm our suspected mechanism and to better understand high-frequency internal waves at glaciers. While we attempted to eliminate calving induced waves in our data processing, some events may have been missed. Confirmation of a turbulent generation mechanism would require an analysis of energy transfers between turbulence and internal waves, which is beyond the scope of this paper. Additionally, wave properties may depend on non-ocean factors such as discharge outlet geometry and terminus geometry which also vary in time.

4.2. How Do Internal Waves Contribute to Boundary Layer Heat and Salt Fluxes?

Within the 3-equation parameterization, the melt rate is proportional to the ocean boundary layer heat and salt fluxes, which are assumed to be linearly dependent on the terminus-parallel ocean velocity (Equation 1 and Text S1 in Supporting Information S1). We consider that the outer velocity may be comprised of plume, mean horizontal and internal wave components denoted by subscript p, subscript m and subscript w respectively, giving,

$$\boldsymbol{u} = (u_m + u_w, 0, w_p + w_w). \tag{2}$$

We have chosen a coordinate system where the second component of velocity is perpendicular to the ice and must satisfy the no-flow condition at the ice-ocean boundary ($v_m = v_w = v_p = 0$) and we neglect the horizontal plume velocity ($u_p = 0$). The contribution of internal waves, plumes and mean flows to melt is the average magnitude of Equation 2 over a wave period T_w, for example,

$$m \propto |\overline{\boldsymbol{u}}| = \frac{1}{T_w}\int_0^{T_w} \sqrt{(u_m + u_w)^2 + (w_p + w_w)^2}\, dt \tag{3}$$

The nonlinearity of Equation 3 ensures that waves always contribute to melting. The significance of the wave contribution will depend on the relative magnitude of waves, plumes and mean flows. Within the discharge plume, large vertical velocities associated with buoyantly rising fluid will dominate other velocity sources ($w_p \gg w_w, u_m, u_w$) and the wave contribution may be negligible. In ambient regions far away from the discharge plume, our observations suggest that waves and mean flows have similar magnitude and both contribute to

melting ($w_w \sim u_w \sim u_m$). For the case of a single sinusoidally varying wave superposed onto a mean flow with $w_w = u_w = u_m$, Equation 3 predicts a 30% increase in the melt rate relative to the case without a wave. In our analysis of melt rate enhancement by waves, we did not include the ambient melt plume velocity since it was not measured, which is equivalent to assuming that $w_p \ll w_w$. In the absence of external flow, this assumption is valid since coupled plume-melt theory predicts weak ambient plume velocities of order 1 cm s^{-1} or less, much weaker than the observed wave velocities (Jackson et al., 2020).

The interaction of plumes, mean flows and waves may involve additional complexities that are not captured by the simplified theory presented here. For instance, enhancement of melt by waves and mean flows might provide additional buoyancy to ambient plumes, increasing their vertical velocity. The combination of a mean and oscillatory boundary layer forcing also occurs in the shallow coastal ocean when currents and surface gravity waves both impinge on the seafloor. In this case, the interaction of surface waves and currents with the bottom boundary layer leads to a higher drag coefficient (Trowbridge & Lentz, 2018, and reference therein). If a similar interaction were to occur at the ice-ocean boundary, it suggests another possible mechanism for increased melt rates via an increased drag coefficient.

Wave-induced melting is likely greatest close to the plume and decreases farther away due to spreading of wave energy. However, complicated glacier geometry could lead to focusing or shadowing in certain regions. Our results suggest that wave energy is concentrated at the pycnocline depth. Consequently, numerical models that do not resolve internal waves may underestimate melting around the pycnocline. In many deep glacial-fjord systems, discharge plumes reach neutral buoyancy below the surface. Atmospheric studies and laboratory tests demonstrate that plumes radiate waves upward into stratified regions implying that discharge-generated waves should also be found close to deep termini (Ansong & Sutherland, 2010; Fovell et al., 1992; Lane et al., 2001; Yue et al., 2013). An uneven vertical distribution of melting, as implied by Figure 4a and implied by the observed melt rates and geometries collected previously in May 2017 (Sutherland et al., 2019), may also lead to uneven glacier shapes that are more prone to calving (Slater et al., 2021). The observed profile of terminus-parallel velocity increases in magnitude toward the surface and could cause melt-induced overcutting, in agreement with observed September 2018 ice morphology (Abib et al., 2023).

5. Conclusion

Our observations reveal the presence of an energetic internal wavefield at Xeitl S´ıt' (LeConte Glacier). Analyses confirm these are generated by the subglacial discharge plume and have the potential to significantly enhance melt rates. Because the fundamental ingredients needed to excite these waves are common to most tidewater glacier systems—an energetic upwelling plume impinging on a stratified ocean—we expect the waves to be widely prevalent at other tidewater glaciers in Greenland, Alaska and Patagonia.

Prior laboratory studies suggest that the internal wave energy flux scales with the plume energy flux (Ansong & Sutherland, 2010) suggesting that more energetic waves may be found at tidewater glaciers with higher discharge rates and more energetic plumes. Our findings highlight the importance of obtaining measurements very close to glaciers, since observations taken far away may miss key dynamical processes and greatly underestimate the energy of ocean flows that can enhance melting. Ultimately, the impact of high-frequency internal waves should be included in parameterizations of melt for accurate modeling of ocean-glacier interactions.

Data Availability Statement

The oceanographic data (ship, autonomous vessel, moorings) are archived at the National Centers for Environmental Information (Accession 0189574, accession.nodc.noaa.gov/0189574). The subglacial discharge data have been archived at the Arctic Data Center (https://doi.org/10.18739/A22G44). The analysis code is available on GitHub (https://github.com/jessecusack/LeConte_plume_internal_waves) and is also permanently archived on Zenodo (https://doi.org/10.5281/zenodo.7682656).

Acknowledgments
These observations were made possible by the talented engineering team who developed the remotely operated vessels and mooring deployment system: Jasmine Nahorniak, June Marion, Nick McComb, Anthony Grana, and Corwin Perren, as well as the Captain and crew of the M/V Amber Anne. We acknowledge the generosity of Teledyne RD Instruments for lending a Sentinel V ADCP despite significant risk of loss. JMC acknowledges the support of a Rutgers EOAS postdoctoral fellowship. This work was supported by NSF OPP Grants 1503910, 1504191, 1504288, 1504521, 2023269, 2023319, and glacial-fjord2023674. ONR Grants N00014-14-1-0490 and N00014-17-1-2864 supported autonomous vessel development. The National Geographic Society Grant CP4-171R-17 supported the design and deployment of the novel system to remotely deploy moorings. We would like to acknowledge high-performance computing support from Cheyenne (https://doi.org/10.5065/D6RX99HX) provided by NCAR's Computational and Information Systems Laboratory, sponsored by NSF.

References

Abib, N., Sutherland, D. A., Amundson, J. M., Duncan, D., Jackson, R. H., Kienholz, C., & Morlighem, M. (2023). Persistent overcut regions dominate the terminus morphology of a rapidly melting tidewater glacier. *Annals of Glaciology*, *41*. https://doi.org/10.1017/aog.2023.38

Amundson, J. M., Kienholz, C., Hager, A. O., Jackson, R. H., Motyka, R. J., Nash, J. D., & Sutherland, D. A. (2020). Formation, flow and break-up of ephemeral ice mélange at LeConte Glacier and Bay, Alaska. *Journal of Glaciology*, *66*(258), 577–590. https://doi.org/10.1017/jog.2020.29

Ansong, J. K., & Sutherland, B. R. (2010). Internal gravity waves generated by convective plumes. *Journal of Fluid Mechanics*, *648*, 405–434. https://doi.org/10.1017/S0022112009993193

Bourgault, D., Janes, D. C., & Galbraith, P. S. (2011). Observations of a large-amplitude internal wave train and its reflection off a steep slope. *Journal of Physical Oceanography*, *41*(3), 586–600. https://doi.org/10.1175/2010JPO4464.1

Carroll, D., Sutherland, D. A., Hudson, B., Moon, T., Catania, G. A., Shroyer, E. L., et al. (2016). The impact of glacier geometry on meltwater plume structure and submarine melt in Greenland fjords. *Geophysical Research Letters*, *43*(18), 9739–9748. https://doi.org/10.1002/2016GL070170

Chambers, D. P., Cazenave, A., Champollion, N., Dieng, H., Llovel, W., Forsberg, R., et al. (2017). Evaluation of the global mean sea level budget between 1993 and 2014. *Surveys in Geophysics*, *38*(1), 309–327. https://doi.org/10.1007/s10712-016-9381-3

Clark, T. L., Hauf, T., & Kuettner, J. P. (1986). Convectively forced internal gravity waves: Results from two-dimensional numerical experiments. *Quarterly Journal of the Royal Meteorological Society*, *112*(474), 899–925. https://doi.org/10.1002/qj.49711247402

Cowton, T., Slater, D., Sole, A., Goldberg, D., & Nienow, P. (2015). Modeling the impact of glacial runoff on fjord circulation and submarine melt rate using a new subgrid-scale parameterization for glacial plumes. *Journal of Geophysical Research: Oceans*, *120*(2), 796–812. https://doi.org/10.1002/2014JC010324

Dohan, K., & Sutherland, B. R. (2005). Numerical and laboratory generation of internal waves from turbulence. *Dynamics of Atmospheres and Oceans*, *40*(1–2), 43–56. https://doi.org/10.1016/j.dynatmoce.2004.10.004

Farmer, D., & Armi, L. (1999). Stratified flow over topography: The role of small-scale entrainment and mixing in flow establishment. *Proceedings of the Royal Society of London. Series A: Mathematical, Physical and Engineering Sciences*, *455*(1989), 3221–3258. https://doi.org/10.1098/rspa.1999.0448

Farmer, D., & Smith, J. D. (1978). Nonlinear internal waves in a fjord. In J. C. J. Nihoul (Ed.), *Elsevier Oceanography Series* (Vol. 23, pp. 465–493). Elsevier. https://doi.org/10.1016/S0422-9894(08)71294-7

Ferrari, R., & Wunsch, C. (2009). Ocean circulation kinetic energy: Reservoirs, sources, and sinks. *Annual Review of Fluid Mechanics*, *41*(1), 253–282. https://doi.org/10.1146/annurev.fluid.40.111406.102139

Fovell, R., Durran, D., & Holton, J. R. (1992). Numerical simulations of convectively generated stratospheric gravity waves. *Journal of the Atmospheric Sciences*, *49*(16), 1427–1442. https://doi.org/10.1175/1520-0469(1992)049⟨1427:NSOCGS⟩2.0.CO;2

Fried, M. J., Carroll, D., Catania, G. A., Sutherland, D. A., Stearns, L. A., Shroyer, E. L., & Nash, J. D. (2019). Distinct frontal ablation processes drive heterogeneous submarine terminus morphology. *Geophysical Research Letters*, *46*(21), 12083–12091. https://doi.org/10.1029/2019GL083980

Fried, M. J., Catania, G. A., Bartholomaus, T. C., Duncan, D., Davis, M., Stearns, L. A., et al. (2015). Distributed subglacial discharge drives significant submarine melt at a Greenland tidewater glacier. *Geophysical Research Letters*, *42*(21), 9328–9336. https://doi.org/10.1002/2015GL065806

Gill, A. E. (1984). On the behavior of internal waves in the wakes of storms. *Journal of Physical Oceanography*, *14*(7), 1129–1151. https://doi.org/10.1175/1520-0485(1984)014⟨1129:otboiw⟩2.0.co;2

Gillibrand, P. A., & Amundrud, T. L. (2007). A numerical study of the tidal circulation and buoyancy effects in a Scottish fjord: Loch Torridon. *Journal of Geophysical Research*, *112*(C5), C05030. https://doi.org/10.1029/2006JC003806

Holland, D. M., & Jenkins, A. (1999). Modeling thermodynamic ice–ocean interactions at the base of an ice shelf. *Journal of Physical Oceanography*, *29*(8), 1787–1800. https://doi.org/10.1175/1520-0485(1999)029⟨1787:MTIOIA⟩2.0.CO;2

Jackson, R. H., Motyka, R. J., Amundson, J. M., Abib, N., Sutherland, D. A., Nash, J. D., & Kienholz, C. (2022). The relationship between submarine melt and subglacial discharge from observations at a tidewater glacier. *Journal of Geophysical Research: Oceans*, *127*(10), e2021JC018204. https://doi.org/10.1029/2021JC018204

Jackson, R. H., Nash, J. D., Kienholz, C., Sutherland, D. A., Amundson, J. M., Motyka, R. J., et al. (2020). Meltwater intrusions reveal mechanisms for rapid submarine melt at a tidewater glacier. *Geophysical Research Letters*, *47*(2), e2019GL085335. https://doi.org/10.1029/2019GL085335

Jackson, R. H., Shroyer, E. L., Nash, J. D., Sutherland, D. A., Carroll, D., Fried, M. J., et al. (2017). Near-glacier surveying of a subglacial discharge plume: Implications for plume parameterizations. *Geophysical Research Letters*, *44*(13), 6886–6894. https://doi.org/10.1002/2017GL073602

Jackson, R. H., Straneo, F., & Sutherland, D. A. (2014). Externally forced fluctuations in ocean temperature at Greenland glaciers in non-summer months. *Nature Geoscience*, *7*(7), 503–508. https://doi.org/10.1038/ngeo2186

Jansson, P., Hock, R., & Schneider, T. (2003). The concept of glacier storage: A review. *Journal of Hydrology*, *282*(1–4), 116–129. https://doi.org/10.1016/S0022-1694(03)00258-0

Jenkins, A. (2011). Convection-driven melting near the grounding lines of ice shelves and tidewater glaciers. *Journal of Physical Oceanography*, *41*(12), 2279–2294. https://doi.org/10.1175/JPO-D-11-03.1

Kienholz, C., Amundson, J. M., Motyka, R. J., Jackson, R. H., Mickett, J. B., Sutherland, D. A., et al. (2019). Tracking icebergs with time-lapse photography and sparse optical flow, LeConte Bay, Alaska, 2016-2017. *Journal of Glaciology*, *65*(250), 195–211. https://doi.org/10.1017/jog.2018.105

Kuettner, J. P., Hildebrand, P. A., & Clark, T. L. (1987). Convection waves: Observations of gravity wave systems over convectively active boundary layers. *Quarterly Journal of the Royal Meteorological Society*, *113*(476), 445–467. https://doi.org/10.1002/qj.49711347603

Lane, T. P., Reeder, M. J., & Clark, T. L. (2001). Numerical modeling of gravity wave generation by deep tropical convection. *Journal of the Atmospheric Sciences*, *58*(10), 1249–1274. https://doi.org/10.1175/1520-0469(2001)058⟨1249:NMOGWG⟩2.0.CO;2

Luckman, A., Benn, D. I., Cottier, F., Bevan, S., Nilsen, F., & Inall, M. (2015). Calving rates at tidewater glaciers vary strongly with ocean temperature. *Nature Communications*, *6*(1), 8566. https://doi.org/10.1038/ncomms9566

Ma, Y., & Bassis, J. N. (2019). The effect of submarine melting on calving from marine terminating glaciers. *Journal of Geophysical Research: Earth Surface*, *124*(2), 334–346. https://doi.org/10.1029/2018JF004820

MacKinnon, J. A., Alford, M. H., Ansong, J. K., Arbic, B. K., Barna, A., Briegleb, B. P., et al. (2017). Climate Process Team on internal-wave driven ocean mixing. *Bulletin of the American Meteorological Society*, *98*(11), 2429–2454. https://doi.org/10.1175/BAMS-D-16-0030.1

Magorrian, S. J., & Wells, A. J. (2016). Turbulent plumes from a glacier terminus melting in a stratified ocean. *Journal of Geophysical Research: Oceans*, *121*(7), 4670–4696. https://doi.org/10.1002/2015JC011160

McConnochie, C. D., & Kerr, R. C. (2017). Testing a common ice-ocean parameterization with laboratory experiments. *Journal of Geophysical Research: Oceans*, *122*(7), 5905–5915. https://doi.org/10.1002/2017JC012918

Melet, A., Hallberg, R., Legg, S., & Polzin, K. (2013). Sensitivity of the ocean state to the vertical distribution of internal-tide-driven mixing. *Journal of Physical Oceanography*, *43*(3), 602–615. https://doi.org/10.1175/JPO-D-12-055.1

Mercenier, R., Lüthi, M. P., & Vieli, A. (2020). How oceanic melt controls tidewater glacier evolution. *Geophysical Research Letters*, *47*(8), 1–9. https://doi.org/10.1029/2019GL086769

Meredith, M. P., Inall, M. E., Brearley, J. A., Ehmen, T., Sheen, K., Munday, D., et al. (2022). Internal tsunamigenesis and ocean mixing driven by glacier calving in Antarctica. *Science Advances*, *8*(47), 1–11. https://doi.org/10.1126/sciadv.add0720

Moffat, C. (2014). Wind-driven modulation of warm water supply to a proglacial fjord, Jorge Montt Glacier, Patagonia. *Geophysical Research Letters*, *41*(11), 3943–3950. https://doi.org/10.1002/2014GL060071

Morton, B., Taylor, G., & Turner, J. S. (1956). Turbulent gravitational convection from maintained and instantaneous sources. *Proceedings of the Royal Society of London. Series A. Mathematical and Physical Sciences*, *234*(1196), 1–23. https://doi.org/10.1098/rspa.1956.0011

Mouginot, J., Rignot, E., Bjørk, A. A., van den Broeke, M., Millan, R., Morlighem, M., et al. (2019). Forty-six years of Greenland Ice Sheet mass balance from 1972 to 2018. *Proceedings of the National Academy of Sciences of the United States of America*, *116*(19), 9239–9244. https://doi.org/10.1073/pnas.1904242116

Nash, J. D., Marion, J., McComb, N., Nahorniak, J., Jackson, R., Perren, C., et al. (2017). Autonomous CTD profiling from the Robotic Oceanographic Surface Sampler. *Oceanography*, *30*(2), 110–112. https://doi.org/10.5670/oceanog.2017.229

Nash, J. D., & Moum, J. N. (2005). River plumes as a source of large-amplitude internal waves in the coastal ocean. *Nature*, *437*(7057), 400–403. https://doi.org/10.1038/nature03936

Rignot, E., Fenty, I., Xu, Y., Cai, C., & Kemp, C. (2015). Undercutting of marine-terminating glaciers in West Greenland. *Geophysical Research Letters*, *42*(14), 5909–5917. https://doi.org/10.1002/2015GL064236

Rignot, E., & Kanagaratnam, P. (2006). Changes in the velocity structure of the Greenland Ice Sheet. *Science*, *311*(5763), 986–990. https://doi.org/10.1126/science.1121381

Ross, L., Pérez-Santos, I., Valle-Levinson, A., & Schneider, W. (2014). Semidiurnal internal tides in a Patagonian fjord. *Progress in Oceanography*, *129*, 19–34. https://doi.org/10.1016/j.pocean.2014.03.006

Schulz, K., Nguyen, A. T., & Pillar, H. R. (2022). An improved and observationally-constrained melt rate parameterization for vertical ice fronts of marine terminating glaciers. *Geophysical Research Letters*, *49*(18), e2022GL100654. https://doi.org/10.1029/2022GL100654

Shepherd, A., Ivins, E., Rignot, E., Smith, B., van den Broeke, M., Velicogna, I., et al. (2020). Mass balance of the Greenland Ice Sheet from 1992 to 2018. *Nature*, *579*(7798), 233–239. https://doi.org/10.1038/s41586-019-1855-2

Slater, D. A., Benn, D. I., Cowton, T. R., Bassis, J. N., & Todd, J. A. (2021). Calving multiplier effect controlled by melt undercut geometry. *Journal of Geophysical Research: Earth Surface*, *126*(7), 1–17. https://doi.org/10.1029/2021JF006191

Slater, D. A., Carroll, D., Oliver, H., Hopwood, M. J., Straneo, F., Wood, M., et al. (2022). Characteristic depths, fluxes, and timescales for Greenland's tidewater glacier fjords from subglacial discharge-driven upwelling during summer. *Geophysical Research Letters*, *49*(10), e2021GL097081. https://doi.org/10.1029/2021GL097081

Slater, D. A., Nienow, P., Sole, A., Cowton, T., Mottram, R., Langen, P., & Mair, D. (2017). Spatially distributed runoff at the grounding line of a large Greenlandic tidewater glacier inferred from plume modelling. *Journal of Glaciology*, *63*(238), 309–323. https://doi.org/10.1017/jog.2016.139

Slater, D. A., Nienow, P. W., Cowton, T. R., Goldberg, D. N., & Sole, A. J. (2015). Effect of near-terminus subglacial hydrology on tidewater glacier submarine melt rates. *Geophysical Research Letters*, *42*(8), 2861–2868. https://doi.org/10.1002/2014GL062494

Slater, D. A., Straneo, F., Das, S. B., Richards, C. G., Wagner, T. J., & Nienow, P. W. (2018). Localized plumes drive front-wide ocean melting of a Greenlandic tidewater glacier. *Geophysical Research Letters*, *45*(22), 12350–12358. https://doi.org/10.1029/2018GL080763

Straneo, F., & Cenedese, C. (2015). The dynamics of Greenland's glacial fjords and their role in climate. *Annual Review of Marine Science*, *7*(1), 89–112. https://doi.org/10.1146/annurev-marine-010213-135133

Sutherland, D. A., Jackson, R. H., Kienholz, C., Amundson, J. M., Dryer, W. P., Duncan, D., et al. (2019). Direct observations of submarine melt and subsurface geometry at a tidewater glacier. *Science*, *365*(6451), 369–374. https://doi.org/10.1126/science.aax3528

Thornalley, D. J., Oppo, D. W., Ortega, P., Robson, J. I., Brierley, C. M., Davis, R., et al. (2018). Anomalously weak Labrador Sea convection and Atlantic overturning during the past 150 years. *Nature*, *556*(7700), 227–230. https://doi.org/10.1038/s41586-018-0007-4

Trowbridge, J. H., & Lentz, S. J. (2018). The bottom boundary layer. *Annual Review of Marine Science*, *10*(1), 397–420. https://doi.org/10.1146/annurev-marine-121916-063351

White, B. L., & Helfrich, K. R. (2008). Gravity currents and internal waves in a stratified fluid. *Journal of Fluid Mechanics*, *616*, 327–356. https://doi.org/10.1017/S0022112008003984

Wood, M., Rignot, E., Fenty, I., Menemenlis, D., Millan, R., Morlighem, M., et al. (2018). Ocean-induced melt triggers glacier retreat in northwest Greenland. *Geophysical Research Letters*, *45*(16), 8334–8342. https://doi.org/10.1029/2018GL078024

Woodson, C. B. (2018). The fate and impact of internal waves in nearshore ecosystems. *Annual Review of Marine Science*, *10*(1), 421–441. https://doi.org/10.1146/annurev-marine-121916-063619

Yue, J., Hoffmann, L., & Joan Alexander, M. (2013). Simultaneous observations of convective gravity waves from a ground-based airglow imager and the AIRS satellite experiment. *Journal of Geophysical Research: Atmospheres*, *118*(8), 3178–3191. https://doi.org/10.1002/jgrd.50341

References From the Supporting Information

Deardorff, J. W. (1980). Stratocumulus-capped mixed layers derived from a three-dimensional model. *Boundary-Layer Meteorology*, *18*(4), 495–527. https://doi.org/10.1007/BF00119502

Ducros, F., Comte, P., & Lesieur, M. (1996). Large-eddy simulation of transition to turbulence in a boundary layer developing spatially over a flat plate. *Journal of Fluid Mechanics*, *326*, 1–36. https://doi.org/10.1017/s0022112096008221

Goldstein, S. (1931). On the stability of superposed streams of Fluids of different densities. *Proceedings of the Royal Society of London*, *132*(820), 524–548. https://doi.org/10.1098/rspa.1931.0116

Hewitt, I. J. (2020). Subglacial plumes. *Annual Review of Fluid Mechanics*, *52*(1), 145–169. https://doi.org/10.1146/annurev-fluid-010719-060252

IOC, SCOR, & IAPSO. (2010). The international thermodynamic equation of seawater – 2010: Calculation and use of thermodynamic properties. *Intergovernmental Oceanographic Commission, Manuals and Guides* (Vol. *56*).

Skyllingstad, E. D., Paulson, C. A., Pegau, W. S., McPhee, M. G., & Stanton, T. (2003). Effects of keels on ice bottom turbulence exchange. *Journal of Geophysical Research*, *108*(12), 1–16. https://doi.org/10.1029/2002jc001488

Skyllingstad, E. D., Smyth, W. D., & Crawford, G. B. (2000). Resonant wind-driven mixing in the ocean boundary layer. *Journal of Physical Oceanography*, *30*(8), 1866–1890. https://doi.org/10.1175/1520-0485(2000)030⟨1866:RWDMIT⟩2.0.CO;2

Skyllingstad, E. D., Smyth, W. D., Moum, J. N., & Wijesekera, H. (1999). Upper-ocean turbulence during a westerly wind burst: A comparison of large-eddy simulation results and microstructure measurements. *Journal of Physical Oceanography*, *29*(1), 5–28. https://doi.org/10.1175/1520-0485(1999)029⟨0005:UOTDAW⟩2.0.CO;2

Smyth, W. D., Moum, J. N., & Nash, J. D. (2011). Narrowband oscillations in the upper equatorial ocean. Part II: Properties of shear instabilities. *Journal of Physical Oceanography*, *41*(3), 412–428. https://doi.org/10.1175/2010JPO4451.1

Taylor, G. I. (1931). Effect of variation in density on the stability of superposed streams of fluid. *Proceedings of the Royal Society of London*, *132*(820), 499–523. https://doi.org/10.1098/rspa.1931.0115